

# Photoexcitations in the Hubbard model – generalized Loschmidt amplitude analysis of impact ionization in small clusters

C. Watzenböck, M. Wallerberger, L. Ruzicka, P. Worm, K. Held and A. Kauch

*Institute of Solid State Physics, TU Wien, 1040 Vienna, Austria*

(Dated: December 2, 2021)

We study photoexcitations in small Hubbard clusters of up to 12 sites, some of which show an increase of the double occupation after the electric field pulse through impact ionization. Here, the time-dependent electromagnetic field is introduced through a Peierls substitution and the time evolution is calculated by exact diagonalization with commutator-free Magnus integrators. As a tool to better analyze the out-of-equilibrium dynamics, we generalize the Loschmidt amplitude. This way, we are able to resolve which many-body energy eigenstates are responsible for impact ionization and which show pronounced changes in the double occupation and spin energy. This analysis reveals that the loss of spin energy is of little importance for impact ionization. We further demonstrate that, for one-dimensional chains, the optical conductivity has a characteristic peak structure originating solely from vertex corrections.

PACS numbers: 71.27.+a, 71.10.Fd

## I. INTRODUCTION

Light-induced phenomena in strongly correlated systems have gained much attention recently, not only because of the advance in pump-probe laser experiments [1, 2] but also for solar energy conversion [3–11]. The particular advantages of a strong electron-electron interaction for solar energy conversion is a phenomenon called impact ionisation [3, 6–12] that allows for the generation of multiple electron-hole pairs (aka doublons and holons) per photon. This is one way for boosting the efficiency of solar cells beyond the Shockley-Queisser limit [13] of 30–34%. Impact ionization is a genuine non-equilibrium process, which is particularly challenging to describe in theory if electronic correlations are strong, so that weak coupling perturbation theory [3] or the Boltzmann equation [12] cannot be reliably applied. One possibility is to employ nonequilibrium dynamical mean-field theory [6, 7, 14] which treats local correlations non-perturbatively, another route is to study the time evolution directly for small clusters [10, 11, 15, 16]. In Refs. 10 and 11 it was shown by studying nonequilibrium spectral functions and the double occupancy that also in small clusters the effect of impact ionization can occur. It manifests itself in the rise of the double occupancy after the light pulse is already turned off. This effect was found to be enhanced by disorder and next-nearest neighbor hopping [10], but strongly suppressed in the case of a simple one-dimensional chain geometry.

As a tool to study such non-equilibrium dynamics, the Loschmidt amplitude [17] has gained popularity recently. For example, in the field of dynamical quantum phase transitions [18] nonanalyticities in its logarithm correspond to a generalized phase transition in time [19]. The Loschmidt amplitude and the related work distribution function have also been used for studying quantum quenches [20, 21] and impact ionization [11]. The module squared of the Loschmidt amplitude, the Loschmidt echo or fidelity, is used as a measure of time irreversibility and

was measured, as early as 1950, in NMR experiments [22].

In this work, we generalize the Loschmidt amplitude, allowing us to study the non-equilibrium dynamics not only with respect to the energy eigenstates but also to resolve for the spectrum of a second (or third ...) quantity. We further show that there is a clear relation between the Loschmidt amplitude and the non-equilibrium Green's function as well as to the optical conductivity. As an application of the generalized Loschmidt amplitude, we study the dynamics and redistribution of the double occupation and Heisenberg spin energy and its correlation to the many-body energy eigenvalues. We focus on times after the electric field pulse, when impact ionization occurs for some of the 12-site Hubbard clusters but not for others. Surprisingly, the observed impact ionization happens predominately when already at least two doubly occupied sites are present.

In Ref. 10 impact ionization in several 12-site systems was analyzed by studying the double occupancy and spectral functions after an electric pulse. It was conjectured that spin fluctuations compete with impact ionization, which might be the reason why in one-dimensional chains with nearest-neighbor hopping only no impact ionization was found. We find that at least for the considered strong electric field strength, the spin fluctuations do not compete with and thus do not suppress impact ionization. In such chains more of the initial spin-spin correlation survives but the change in Heisenberg spin energy after the pulse is smaller than for the other geometries with a larger connectivity. A further difference between the aforementioned one-dimensional chains and other geometries is that for the chains vertex corrections to the optical conductivity dominate and lead to sharp absorption peaks.

The paper is organized as follows: Section II outlines the used model and gives details on the time-evolution algorithm. In Section III, we introduce the Loschmidt amplitude and show how light absorption can be analyzed with it. We further elaborate on the relation to

Fermi's golden rule. In Section IV the Loschmidt amplitude is expressed in the quantum many body picture and can be partly represented also by means of simple one-particle excitations with the Green's function formalism. We highlight which features are solely due to vertex corrections and thus cannot be captured this way. In Section V, we introduce a novel generalization of the Loschmidt amplitude which can be used to determine which energy states are responsible for the long term dynamics of a desired observable. We apply it in this section to the double occupancy to elucidate the phenomenon of impact ionization. In Section VI we show the spin correlation function and the different energy scales to determine the importance of spin excitations in 12-site systems. We then apply the generalized Loschmidt amplitude to a measure of spin-correlations in Section VII and summarize our findings in Section VIII.

## II. HUBBARD MODEL AND TIME EVOLUTION

### A. Hamiltonian

As a prototypical Hamiltonian for strongly correlated electrons systems we consider the Hubbard model [23], given by

$$\hat{H} = \sum_{i,j,\sigma} v_{ij} \hat{c}_{j\sigma}^\dagger \hat{c}_{i\sigma} + U \sum_i \hat{n}_{i\uparrow} \hat{n}_{i\downarrow}. \quad (1)$$

Here,  $\hat{c}_{i\sigma}^\dagger$  ( $\hat{c}_{i\sigma}$ ) creates (annihilates) an electron on site  $i$  with spin  $\sigma$ ,  $\hat{n}_{i\sigma} = \hat{c}_{i\sigma}^\dagger \hat{c}_{i\sigma}$  is the occupation number operator,  $U$  is the (screened) Coulomb interaction, between electrons on the same site, and  $v_{ij}$  for  $i \neq j$  describes the hopping amplitude from site  $i$  to  $j$ . In the following we assume the system to be half-filled, meaning on average each site has 0.5 spin-up electrons and 0.5 spin-down electrons.

### B. Light pulse

The interaction with light is described by coupling an external, classical electric field pulse  $\vec{E}(t)$  to the system by Peierls substitution [24] in a gauge where  $\vec{E}(t) = -\partial_t \vec{A}(t)$  (sometimes referred to as Weyl gauge). Under Peierls substitution the time dependence enters only as a phase factor in the hopping terms

$$v_{ij} \rightarrow v_{ij} e^{i q \chi_{ij}(t)} = v_{ij} e^{-i \int_{R_i}^{R_j} d\vec{r} \cdot \vec{A}(\vec{r}, t)}. \quad (2)$$

Here, we are working in natural units where the charge of the electron  $q = 1$ , Plank's reduced constant  $\hbar = 1$  and the geometric lattice spacing  $\tilde{a} = 1$ . All energies in this paper are in units of the nearest neighbor hopping term  $|v_{ij}| \equiv 1$ . Typical hopping values in correlated systems

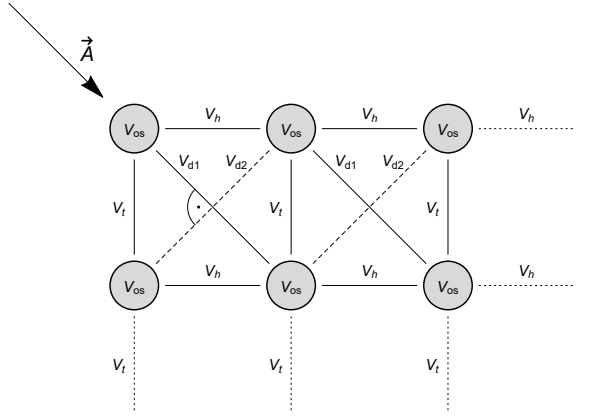


FIG. 1. Example of a  $2 \times 3$  box geometry (possibly further extended) with on-site potential equal on all sites  $v_{ii} = v_{os}$ , NN hopping  $v_h$  in horizontal direction and  $v_t$  in the vertical direction as well as two different NNN (diagonal) hoppings  $v_{d1}$  and  $v_{d2}$ . In our simulations, the time-independent prefactors are equal for NN hoppings  $v_t = v_h \equiv 1$  and for NNN hoppings  $v_{d1} = v_{d2} \equiv v_d$ . The vector potential  $\vec{A}$  is chosen along one of the diagonal directions (as shown in the Figure and employed in our calculation), the parameter  $a$  describing the strength of the field is the same for  $v_h$  and  $v_t$ , it is twice as big for  $v_{d1}$ , and zero for  $v_{d2}$ .

are around 0.5eV, which corresponds to time units of  $\sim 1$  fs.

We also assume that the wavelength of light is much larger than the system size (optical light). Therefore we use a vector potential independent of  $\vec{r}$ . For modeling of the  $\vec{E}$ -field we follow Ref. 10 and choose

$$\vec{A}(t) = \frac{\vec{E}_0}{\omega_p} [\cos(\omega_p(t - t_p)) - \cos(\omega_p t_p)] e^{-\frac{(t - t_p)^2}{2\sigma_p^2}}, \quad (3)$$

which approximately corresponds to an  $\vec{E}$ -field of

$$\vec{E}(t) = \vec{E}_0 \sin(\omega_p(t - t_p)) e^{-\frac{(t - t_p)^2}{2\sigma_p^2}} \quad (4)$$

for  $\omega_p \gg \sigma_p$ . For all the simulations we applied the field in-plane and under a  $45^\circ$  angle, as illustrated in Fig. 1. For convenience we combined the magnitude of the  $E$ -field together with the lattice constant  $\tilde{a}$ , and the frequency of the pulse  $\omega_p$  into a single, direction-dependent parameter  $a \equiv \vec{E}_0 \cdot \vec{e}_x \tilde{a} / \omega_p$ .

### C. Geometries and model parameters of the systems considered

In this work we mainly focus on 12-site systems ( $N_s = 12$ ) of three different geometries:  $4 \times 3$  and  $6 \times 2$  boxes and a  $12 \times 1$  chain. We use open boundary conditions (OBC), i.e., no hopping is possible from the leftmost sites to the left, and from the rightmost sites to the right. Additionally we also considered a  $12 \times 1$  system with periodic

boundary conditions (PBC). We implemented the  $A$ -field for PBC in such a way that it does not break the translation symmetry. Strictly speaking this idealization would not correspond to an electric field, but rather a magnetic field through a closed ring that entails a circular E-field along the ring and does not couple to the spin.

The interaction for the 12-site systems is always set to  $U = 8$ , and for the frequency and field strength we chose, to allow for direct comparisons, the same parameters as in [10], i.e.  $\omega_p = 11$  and  $a = 0.8$ , unless specified otherwise. We also present selected results for an  $8 \times 1$  system, for which we were still able to fully diagonalize the Hamiltonian.

#### D. Time evolution

In order to calculate the time evolution of the system driven out of equilibrium by a time-dependent light pulse, we solve the time-dependent Schrödinger equation

$$i\partial_t |\psi(t)\rangle = \hat{H}(t) |\psi(t)\rangle, \quad |\psi(0)\rangle = |\psi_0\rangle \quad (5)$$

using optimized commutator-free Magnus integrators of fourth order described in detail as CF4oH in Ref. [25]. As an error tolerance for the adaptive time-stepping algorithm we used  $\text{tol} < 10^{-6}$ . The tolerance for the adaptive Lanczos method for the matrix exponential was set to less than  $10^{-8}$ . The initial state  $|\psi_0\rangle$  of the time evolution is always taken to be the (non-degenerate) ground state.

### III. LOSCHMIDT AMPLITUDE AND THE FERMI'S GOLDEN RULE

#### A. Loschmidt amplitude

We use the Loschmidt amplitude to decompose the wave-function  $|\psi\rangle$  with respect to the eigenstates of  $\hat{H}(t_0 = 0)$  [26]

$$L^{|\psi\rangle}(\tau) \equiv \langle\psi| e^{-i\tau\hat{H}(0)} |\psi\rangle, \quad (6)$$

which was also utilized by others [11, 27]. Its Fourier transform has a spectral representation with respect to the eigenstates of  $\hat{H} \equiv \hat{H}(t_0 = 0)$  ( $\hat{H} |E_n\rangle = E_n |E_n\rangle$ ):

$$L^{|\psi\rangle}(\omega) \equiv \int_{-\infty}^{\infty} d\tau e^{i\tau\omega} L^{|\psi\rangle}(\tau) = 2\pi \sum_n |\langle\psi|E_n\rangle|^2 \delta(\omega - E_n), \quad (7)$$

We are interested in the evolution of the Loschmidt amplitude with time. To this end, we use the time evolution operator  $U$  with  $|\psi(t)\rangle = U(t, t_0) |\psi_0\rangle$ , and denote such time-dependent Fourier transform of the Loschmidt amplitude as  $L^{|\psi(t)\rangle}(\omega)$ . In the following, we set the ground-state energy to zero, as it simplifies some subsequent equations.

The major advantage of using the Loschmidt amplitude for describing the systems is that it can be efficiently computed e.g. through time-propagation with commutator free Magnus integrators (or density matrix renormalization group for one-dimensional systems [27]) even if the dimension of the Hamiltonian is so large that it prevents direct diagonalization. After the light-pulse fades away, i.e., for  $t \gg t_p$ , the Loschmidt amplitude is independent of time. For cases where all the eigenstates  $|E_n\rangle$  of the given operator are known one can directly use Eq. (7) to obtain the Loschmidt amplitude. However, for a general operator like the Hamiltonian where the eigenstates are a priori unknown it is advantageous to work directly with Eq. (6).

#### B. Visualizing Fermi's golden rule with Loschmidt amplitude

Using the Loschmidt amplitude we can identify which of the eigenstates of the unperturbed Hamiltonian are excited by the perturbation through the  $A$ -field. For small perturbations, one may resort to a Fermi's golden rule (FGR) description. corresponding in our case to short times, before the pulse in Eq. (3) reaches the full strength, we expect the Fermi's golden rule (FGR) to hold.

To make a connection with FGR we split the Hamiltonian into a static part and a time-dependent perturbation. The static part is given by Eq. (1) with time-independent  $v_{ij}$ . The rest constitutes the dynamic part and may be expanded with respect to  $\vec{A}$  as

$$\hat{H}_{\text{dyn}}(t) = \sum_{ij} (e^{i\chi_{ij}(t)} - 1) v_{ij} \hat{c}_{i\sigma}^\dagger c_{j\sigma} = \vec{J} \cdot \vec{A}(t) + \mathcal{O}(\vec{A}^2) \quad (8)$$

with the current operator

$$\vec{J} = -i \sum_{\sigma} \sum_{ij} (\vec{R}_i - \vec{R}_j) v_{ij} \hat{c}_{i\sigma}^\dagger c_{j\sigma}. \quad (9)$$

For convenience we define the projection of the current  $\vec{J}$  onto the direction of the  $\vec{A}$  field as  $\vec{J} \vec{A}(t) \equiv \hat{j} f(t)$  with  $f(t) = a [\cos(\omega_p(t - t_p)) - \cos(\omega_p t_p)] e^{-\frac{(t-t_p)^2}{2\sigma^2}}$ .

For a large pulse width  $\sigma$  one ends up with a perturbation  $\propto \cos(\omega_p t)$  and one can directly apply the textbook version of Fermi's golden rule according to which the probability amplitude of the transition from an initial state  $|i\rangle$  to a final state  $|f\rangle$  is given by

$$\Gamma_{i \rightarrow f} = 2\pi \left| \langle f | \hat{j} | i \rangle \right|^2 \mathcal{N}(\omega), \quad (10)$$

where  $\mathcal{N}(\omega) = \frac{1}{\dim \mathcal{H}} \sum_n \delta(\omega - E_n)$  is the *density of states* of the system and  $E_n$  are the many-body eigenenergies [28]. Please note that this version of FGR requires a long time  $t \gg 1/\omega_p$ , but at the same time a weak perturbation which for our  $A$ -field strength translates in a not too long time.

A simple way of visualizing which final states are allowed within the first order perturbation theory (FGR) is by means of the Fourier transform of the Loschmidt amplitude with respect to the wave function  $\hat{j}|\psi_0\rangle$ :

$$L^{\hat{j}|\psi_0\rangle}(\tau) = \langle\psi_0|\hat{j}e^{-i\tau\hat{H}}\hat{j}|\psi_0\rangle. \quad (11)$$

We will further refer to this function as the Loschmidt amplitude for optical absorption for reasons that will become clear later in Section IV. The Fourier transform reads then

$$L^{\hat{j}|\psi_0\rangle}(\omega) = 2\pi \sum_n \left| \langle E_n | \hat{j} | \psi_0 \rangle \right|^2 \delta(\omega - E_n), \quad (12)$$

and is just given by a sum over the possible final states of Eq. (10).

### 1. $8 \times 1$ system

In Fig. 2, we show the Loschmidt amplitude given by Eq. (7),  $L^{|\psi(t)\rangle}(\omega)$ , as well as the FGR-allowed transitions given by  $L^{\hat{j}|\psi_0\rangle}(\omega)$  of Eq. (11) for an  $8 \times 1$  system at two different times:  $t = 4.5$  (at the onset of the EM pulse that is centered at  $t_p = 8$ ) and  $t = 20$ .

At small times (or small electric fields) only transitions allowed by  $L^{\hat{j}|\psi_0\rangle}(\omega)$  are possible, which is clearly visible in the top panel of Fig. 2. The maximal absorption rates can only be achieved when the pulse frequency  $\omega_p$  has a large overlap, or resonance, with the allowed states. The Fourier transform of the electric field (in arbitrary units) is also shown in Fig. 2 as a gray curve centered around  $\omega_p = 6$  with  $\sigma_p = 2$ . For the allowed transitions we find a distinct peak structure. A more detailed description of the peaks can be found later in Section IV. Also the many-body density of states  $\mathcal{N}(\omega)$  is shown with a broad distribution of eigenstates. This is due to the rather weak interaction of  $U = 4$ . For large interaction values, closer to the atomic limit, the density of states will only have contributions around  $Un$  with  $n \in \mathbb{N}_0$ , where each contribution can be associated with a specific double occupation value.

The Loschmidt amplitude  $L^{|\psi(t)\rangle}(\omega)$  for a later time,  $t = 20$  can no longer be described by the FGR (see lower panel of Fig. 2). When the energy levels given by  $L^{\hat{j}|\psi_0\rangle}(\omega)$  are at least partially occupied the pulse can excite the system further. If higher energy states are available and allowed by the selection rules the predominant excitations are around integer multiples of the pulse frequency  $\omega_p$ . One may refer to these as single-, double- and triple-photon excitations, although the electric field was treated as classical. The multi-photon excitations in this sense are, however, found to be retarded with respect to the single photon excitations, signifying sequential absorption (see also Fig. 3(b)-(f)).

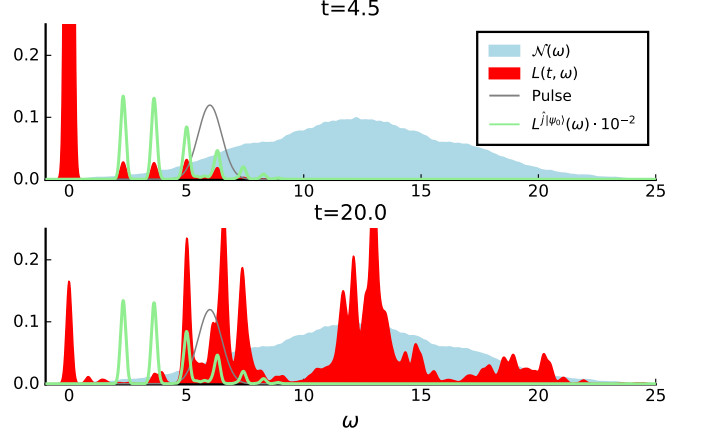


FIG. 2. Density of states  $\mathcal{N}(\omega)$  and Loschmidt amplitude  $L(t, \omega)$  for a  $8 \times 1$  geometry with  $U=4$  NN-hopping only. The light-green line ( $L^{\hat{j}|\psi_0\rangle}$ ) shows the allowed transitions by first order perturbation theory from the ground state. The gray curve ("Pulse") shows the Fourier-transform of the  $A$ -field in arbitrary units, which has a base frequency  $\omega_p = 6$  maximal amplitude at time  $t_p = 8$  and pulse width  $\sigma_p = 2$ .

### 2. 12-site systems

Motivated by the study of Refs. [10, 11], where impact ionization was found to occur in  $4 \times 3$  and  $6 \times 2$  clusters, but not in the  $12 \times 1$  chains, we analyzed these systems in more detail. For the  $12 \times 1$  systems we considered both open and periodic boundary conditions (OBC and PBC). For the chains with OBC we considered systems with nearest-neighbour (NN) hopping only as well as a frustrated system with next-nearest-neighbour (NNN) hopping  $v' = 0.5$ . These systems were chosen to investigate the role of spin frustration, which we discuss later in Sections VI and VII.

In Fig. 3(a) we show the FGR-allowed transitions for all considered 12-site systems. They all show a similar gap of  $\gtrsim 4.8v$  and in all systems the bandwidth is approximately equal to 8 (in the units of NN hopping, as defined in Section II B). Similar as for the  $8 \times 1$  case,  $L^{\hat{j}|\psi_0\rangle}(\omega)$  comprises a small number of sharp peaks for the chains with NN-hopping only. For the chain with PBC the sharp absorption peaks are fewer and have larger weight than for OBC as this system has more symmetries. There are more peaks for the other systems, which visually form a band. All peaks shown here and in later plots (unless mentioned otherwise) are broadened with  $\sigma_\omega = 0.09$ , meaning that a delta-peak in frequency is depicted as a Gaussian with standard-deviation  $\sigma_\omega$ .

The full time-dependent Loschmidt amplitude  $L^{|\psi(t)\rangle}(\omega)$  is shown in Fig. 3 (b)-(f) for different times (color range from blue to orange), together with  $L^{\hat{j}|\psi_0\rangle}(\omega)$  (light green). For the shortest time, at the onset of the pulse, only the transitions present in  $L^{\hat{j}|\psi_0\rangle}(\omega)$  (allowed by FGR) are visible. For later times, the applied  $E$ -field is large enough to generate

a strong out-of equilibrium state. During the pulse there are excitations for almost for all energies in the range shown. After the pulse is over all systems show pronounced weights at  $\omega_p = 11$ ,  $2\omega_p$  and  $3\omega_p$ , which we can describe as (sequential) single- double- and triple photon excitations.

#### IV. CONNECTION BETWEEN GREEN'S FUNCTION AND THE LOSCHMIDT AMPLITUDE

For extended systems an exact diagonalization, which accurately captures all allowed transitions, is unfeasible. In this case one often uses Green's function based methods (with Feynman diagrammatics) to predict or describe optical absorption. The Loschmidt amplitude for optical absorption can also be expressed in this language.

*Diagrammatic expansion of  $L^{\hat{j}|\psi_0\rangle}(\omega)$*  – The greater and lesser Green's functions are defined as [30, Ch. 3]

$$\begin{aligned} G_{ij}^>(t,0) &= -i \langle \hat{c}_i(t) \hat{c}_j^\dagger(0) \rangle \\ G_{ij}^<(t,0) &= i \langle \hat{c}_j^\dagger(0) \hat{c}_i(t) \rangle. \end{aligned} \quad (13)$$

The other common one-particle Green's functions (retarded-, advanced- or Keldysh-) can be constructed from the lesser and greater Green's functions by linear combinations.

We now turn to the diagrammatic expansion of the current-current correlation function  $\langle \hat{j}(t)j(0) \rangle$ . We express the current operator projected onto the  $\vec{A}$ -field through the creation and annihilation operators as  $\hat{j} \equiv \sum_{ij} \gamma_{ij} \hat{c}_i^\dagger \hat{c}_j$ . To utilize Wick's theorem, the current-current correlation function may be transformed into a contour-ordered string of operators on the Schwinger-Keldysh contour via the closed time-path contour formalism [30, 31]. This leads to

$$\begin{aligned} \langle \hat{j}(t)j(0) \rangle &= \text{Tr} \hat{\rho}_0 \mathcal{T}_C e^{-i \int_C d\tau \hat{H}'(\tau)} \hat{j}^{[+]}(0) \hat{j}^{[-]}(t) \\ &= \sum_{ijij'} \gamma_{ij} \gamma_{i'j'} \text{Tr} \hat{\rho}_0 \mathcal{T}_C e^{-i \int_C d\tau \hat{H}'(\tau)} \\ &\quad \hat{c}_i^{[+]}(0^+) \hat{c}_j^{[+]} \hat{c}_{i'}^{[-]}(t+0^+) \hat{c}_{j'}^{[-]}(t), \end{aligned} \quad (14)$$

in the notation of [30, Ch. 4.3.2]. That is, the superscript indices  $[+]/[-]$  denote the Schwinger-Keldysh forward/backward contour and  $0^+$  denotes  $\lim_{\epsilon \rightarrow 0; \epsilon > 0} \epsilon$ ; The

perturbation  $H'(\tau)$  is the interacting part of the Hamiltonian together with the external perturbation in the interaction picture with respect to the kinetic term  $\sum_{ij\sigma} v_{ij}(t=0) \hat{c}_{i\sigma}^\dagger \hat{c}_{i\sigma}$  acting as the unperturbed reference. The disconnected contraction of Wicks theorem vanishes as the current expectation value is zero without an external field. The other resulting terms can then be distributed into the bubble term (with a full Green's function) and vertex corrections.

$$\begin{aligned} \langle \hat{j}(t)j(0) \rangle &= \sum_{ijij'} \gamma_{ij} \gamma_{i'j'} G_{j'i}^>(t,0) G_{i'j}^<(0,t) \\ &\quad + \text{(vertex corrections)}. \end{aligned} \quad (15)$$

For a time-independent Hamiltonian we can rearrange Eq. (11) and express the Loschmidt amplitude for the absorption as

$$L^{\hat{j}|\psi_0\rangle}(t) = \langle \psi_0 | \hat{j}(t)j(0) | \psi_0 \rangle, \quad (16)$$

where we inserted  $\mathbf{1} = e^{-it\hat{H}} e^{it\hat{H}}$  with  $\hat{H} = \hat{H}(t=0)$  before the first current operator and set the ground-state energy to zero. Notice that for an arbitrary state (or more general a mixture of states) modifications to the above expression would be necessary.

The leading order terms (in  $\vec{A}$ ) for a diagrammatic expansion of the Loschmidt amplitude for optical absorption is thus given by

$$\begin{aligned} L^{\hat{j}|\psi_0\rangle}(t) &= \sum_{ijij'} \gamma_{ij} \gamma_{i'j'} G_{j'i}^>(t) G_{i'j}^<(-t) \\ &\quad + \text{(vertex corrections)} + \mathcal{O}(\vec{A}) \end{aligned} \quad (17)$$

where  $G_{ij}^<(t)/G_{ij}^>(t)$  is the lesser/greater equilibrium Green's function. The above expression links the FGR-given absorption at short times with the quasiparticle picture of Refs. [10, 11], where the description using the one-particle Green's function (spectral function) was used to discuss the presence or absence of impact ionization. In this Green's function based quasiparticle picture light can be absorbed only if the pulse frequency is larger than the gap and smaller than the total bandwidth of the spectral function. This approach corresponds to taking only the bubble contribution into account. In the following we analyze for which systems such an approach fails.

In Fig. 4 we show the full Loschmidt amplitude for absorption  $L^{\hat{j}|\psi_0\rangle}$  together with the bubble contribution (first term in Eq. (17)) for the  $8 \times 1$  systems with different interaction values. In the case of  $U = 0$  there are no vertex corrections and the bubble contribution is equal to the full function. In all other cases the vertex corrections change the result quite significantly. What is described reasonably well already by the bubble term (and thus by the quasiparticle picture) is the size of the gap and the bandwidth. The vertex corrections lead to a slight narrowing of the bandwidth and also to a slightly larger gap. However, the sharp, almost equally spaced peaks in the full  $L^{\hat{j}|\psi_0\rangle}(\omega)$  are described only by inclusion of vertex corrections. The bubble term completely fails to reproduce the correct position of the peaks as well as their weight.

The almost equal-distance distribution of the absorption peaks can be understood by looking at the one-dimensional systems at strong coupling. As discussed e.g. by Lyo *et al.* [29], the major contribution to the photoabsorption is given by the following process: At half filling in the large  $U$  limit each site is occupied by exactly one electron. Incoming light can create through the current operator a hole and a double occupancy at a neighboring site. The hole and the double occupancy (doublon) can subsequently propagate through the system. The doublon-hole pair has a total momentum of

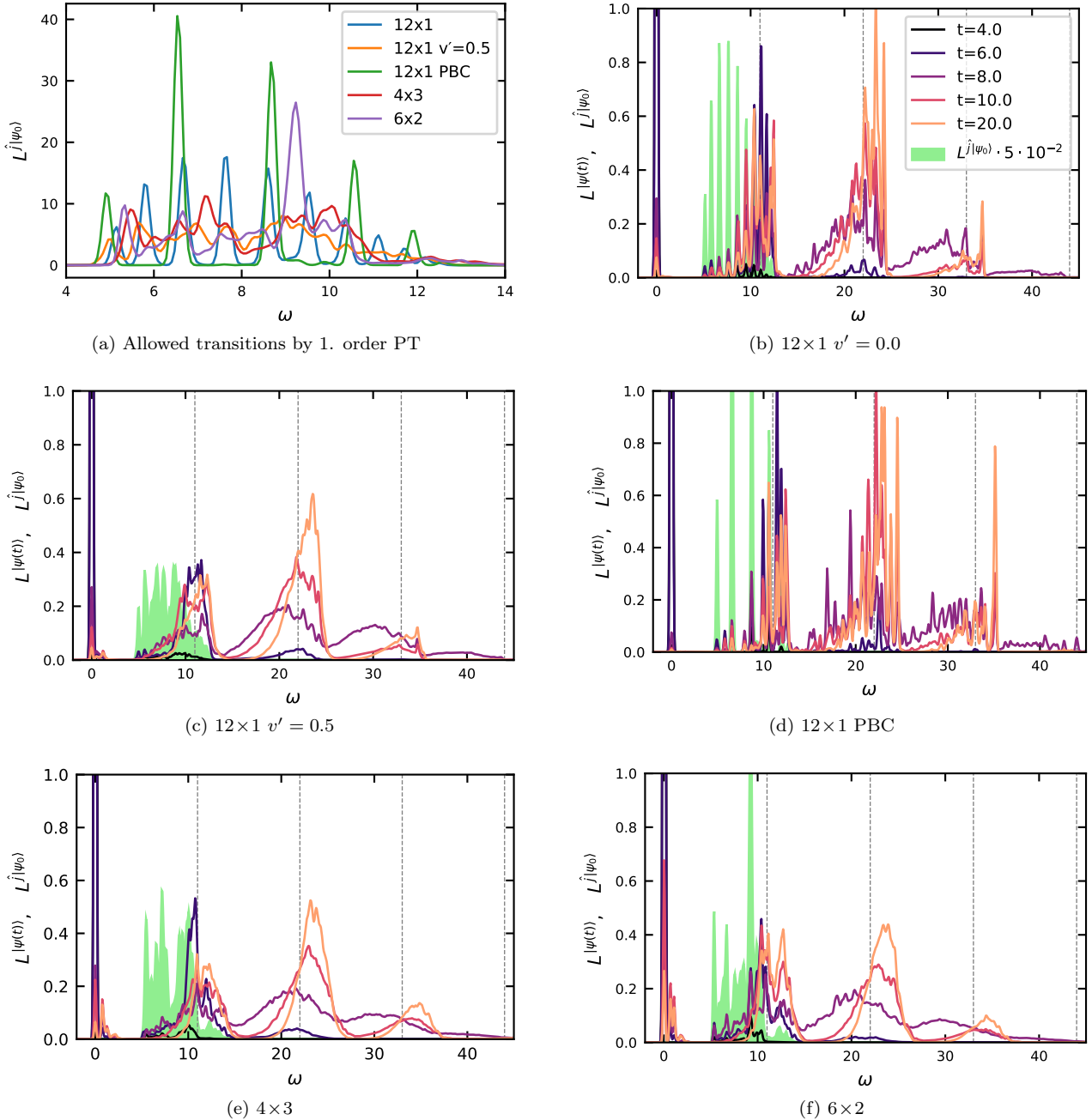


FIG. 3. Allowed transitions by first order perturbation theory  $L^{\hat{j}|\psi_0\rangle}(\omega)$  and time resolved Loschmidt amplitude  $L^{|\psi(t)\rangle}(\omega)$  for different  $N_s=12$  systems. In (a) only  $L^{\hat{j}|\psi_0\rangle}(\omega)$  is shown for all systems. In (b)-(f)  $L^{|\psi(t)\rangle}(\omega)$  is shown for the five  $N_s=12$  systems at several times during the pulse (centered at  $t_p = 8$ ) and after it. The dashed gray lines mark integer multiples of the pulse frequency  $\omega_p$ . After  $t = 20$   $L^{|\psi(t)\rangle}(\omega)$  does not change any more. The legend for (c)-(f) is the same as for (b).

zero. The doublon and the hole each carry a momentum of  $k$ , which takes only several discrete values for small chains. These values are reflected in the different peaks visible in the absorption spectrum. Lyo et al. [29] showed that for the large  $U$  limit in the antiferromagnetic phase the optical conductivity (which is directly related to the Loschmidt amplitude; see next paragraph) has in one di-

mention the following form

$$\sigma^R(\omega) = \frac{4\pi v^2}{\omega} \sum_k \sin^2(k) \delta(U - 4v \cos(k) - \omega) \quad (18)$$

where  $k$  is the momentum of the doublon-hole pair and  $v$  is the NN hopping (set to 1 in this paper). For PBC the allowed momenta are  $k = \frac{2\pi n}{N_s}$  where  $n \in [0, N_s - 1]$ . For

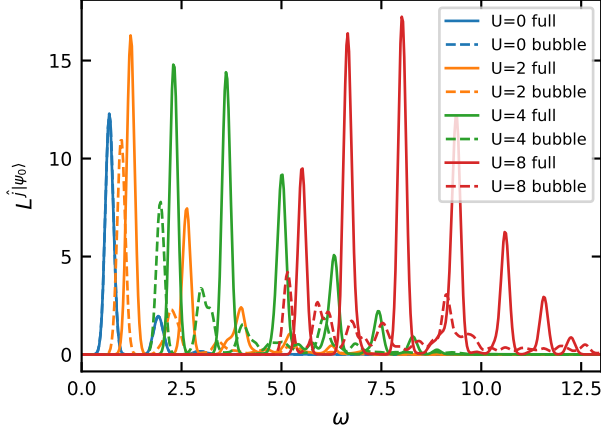


FIG. 4. Optical absorption given by  $L^{j|\psi_0\rangle}(\omega)$  for an  $8 \times 1$  system with NN hopping, together with the static bubble contribution (only the first term in Eq. (17) with  $\vec{A} = 0$ ) for several values of the interaction  $U$ . For  $U = 0$  the bubble contribution matches the full  $L^{j|\psi_0\rangle}(\omega)$  exactly (no vertex corrections).

OBC we have instead  $k = \frac{\pi n}{N_s}$  which corresponds to more different energies. This explains why there are twice as many peaks for OBC as for PBC in Fig. 3(a).

In the top panel of Fig. 5 we show  $L^{j|\psi_0\rangle}(\omega)$  (bubble and full), together with the from Eq. (18) predicted peak positions for the  $N_s = 12$  Hubbard chain, for  $U = 8$  for both OBC and PBC. Again we see that although the gap and bandwidth are well reproduced by the bubble contribution (dashed lines in Fig. 5), the sharp peak structure is completely determined by the vertex corrections (blue and orange full lines in Fig. 5). Also the optical spectral weight is considerably enhanced by vertex corrections. The analytical results of Lyo et. al do not, in this case, give the correct gap size. They would predict a gap of  $U - 4$  without finite size effects. For a 12-site system with PBC the gap is predicted to be  $U - 3.46$  since for  $k = 0$  the matrix element (sine function in Eq. (18)) is zero. For our PBC results the lowest  $\omega$  for which the system can absorb energy is larger:  $\omega = 4.9$  (for OBC it is 5.15, also larger than the predicted value of  $U - 3.86$ ). The difference is not solely due to the not fully applicable large  $U$  expansion as also for larger  $U$  values we do not get the predicted gap (see Appendix C where the results for  $U = 8 \cdot 2^n$  for  $n \in [0, 1, 2, 3]$  are shown in Fig. 12 and a brief explanation is given). The overall structure of the spectrum is however well reflected by the approximate expression in Eq. (18).

In the bottom panel of Fig. 5 we show the bubble contribution (dashed lines) and full  $L^{j|\psi_0\rangle}(\omega)$  (full lines) for 12-site systems with higher connectivity. Contrary to the case of NN-hopping chains shown in the top panel, the full spectrum does not consist of few well separated peaks. However, also here the vertex corrections contain

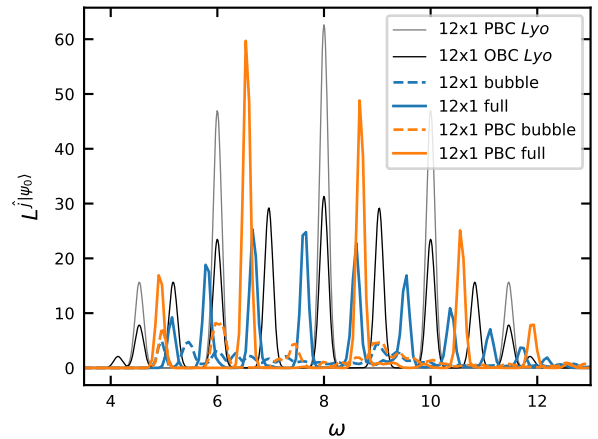


FIG. 5. Optical absorption given by  $L^{j|\psi_0\rangle}(\omega)$  (full lines) and its bubble contribution only (first term in Eq. (17), dashed lines) for  $N_s = 12$  systems. Top panel:  $12 \times 1$  chain with OBC and PBC together with the approximate analytical results by Lyo et. al [29] (black and gray lines). Bottom panel:  $4 \times 3$ ,  $6 \times 2$ , and  $12 \times 1$  with NNN hopping of  $v' = 0.5$  and OBC.

large weight that is differently distributed than in the bubble and there are additional peaks stemming solely from vertex corrections. The gap and bandwidth are already well predicted by the bubble part, although the gap is slightly larger when vertex corrections are included.

*Connection to optical conductivity* – There is an intimate relationship between the retarded current-current correlation function  $K^R(t, t')$  and the Loschmidt amplitude  $L^{j|\psi_0\rangle}$ . The former gives an answer to the question how current responds to the perturbation of the system with a classical  $E$ -field within linear response theory. The latter answers the question at which energies the system can absorb energy in the lowest order perturbation theory in  $E$ . They are related as

$$\begin{aligned} K^R(t, 0) &= i\theta(t) \langle [\hat{j}(t), \hat{j}(0)] \rangle_0 \\ &= -2\theta(t) \Im L^{j|\psi_0\rangle}(t). \end{aligned} \quad (19)$$

Note that for an arbitrary initial state (not the ground state used here) this relation will have to be modified. We show in the Appendix A that in frequencies the (antisymmetric) imaginary part of the retarded current-current correlation function is for positive frequencies exactly twice the Loschmidt amplitude for the state  $\hat{j}|\psi\rangle_0$ :

$$L^{\hat{j}|\psi\rangle_0}(\omega > 0) = 2 \Im K^R(\omega > 0) \quad (20)$$

## V. GENERALIZED LOSCHMIDT AMPLITUDE FOR THE DOUBLE OCCUPANCY AND ENERGY

In the previous chapter the Loschmidt amplitude  $L_{\hat{A}}^{|\psi\rangle}$  was interpreted as a spectral decomposition of the state  $|\psi\rangle$  with respect to the eigenstates of  $\hat{A}$ . The most prominent example being  $\hat{A} = \hat{H}(0)$ . We now want to generalize this concept and decompose the state with respect to two operators at the same time. This corresponds to the joint probability distribution of  $\hat{A}$  and  $\hat{B}$  where  $\hat{B}^\dagger = \hat{B}$  and reads as

$$L_{AB}^{|\psi\rangle}(\bar{\alpha}, \bar{\beta}) \equiv \langle \psi | e^{-i\bar{\alpha}\hat{A}} e^{-i\bar{\beta}\hat{B}} | \psi \rangle. \quad (21)$$

The Fourier transform of Eq. (21) with respect to  $\bar{\alpha} \rightarrow \alpha$  and  $\bar{\beta} \rightarrow \beta$  is given by

$$L_{AB}^{|\psi\rangle}(\alpha, \beta) = (2\pi)^2 \sum_a \sum_b \langle \psi | a \rangle \langle a | b \rangle \langle b | \psi \rangle \times \delta(\beta - b) \delta(\alpha - a), \quad (22)$$

where  $\hat{A}|a\rangle = a|a\rangle$  and  $\hat{B}|b\rangle = b|b\rangle$ . An extension to more than two operators is straightforward, though computationally unfeasible. If the operators  $\hat{A}$ ,  $\hat{B}$  do not commute  $L_{AB}^{|\psi\rangle}(\alpha, \beta)$  is a complex quantity. For the interpretation as a probability distribution the real part is sufficient (see Appendix A).

In the context of impact ionization it is interesting to know which energy-states are responsible for the long-time dynamics of the double occupancy after the  $E$ -field pulse is over. To this end we consider  $\hat{A} = \hat{H}(0)$  and  $\hat{B} = \hat{D} \equiv \sum_i \hat{n}_{\uparrow i} \hat{n}_{\downarrow i}$ . The double-occupancy operator  $\hat{D}$  has the eigenvalues  $EV(\hat{D}) = \{0, 1, \dots, N_s/2\}$  for half-filling. This leads to

$$L_{\hat{H}\hat{D}}^{|\psi(t)\rangle}(\omega, D) = (2\pi)^2 \sum_n \sum_m \langle \psi(t) | E_n \rangle \langle E_n | D_m \rangle \times \langle D_m | \psi(t) \rangle \delta(\omega - E_n) \delta(D - D_m). \quad (23)$$

During the pulse the Hamiltonian is time-dependent and spectral weight can be shifted between different eigenvalues of  $\hat{H}$  (named  $EV(\hat{H})$ ). In Fig. 6(a) we show the real part of the generalized Loschmidt amplitude  $L_{\hat{H}\hat{D}}^{|\psi(t)\rangle}(t, \omega, D)$  for a time  $t = 100$  long after the pulse. We find an almost linear relationship between the double-occupancy eigenvalues and the eigenenergies with a slope which is close to the strong-coupling limit of  $1/U$ .

After the pulse (centered at  $t_p = 8$ ) the Hamiltonian is time independent and the  $L(t, \omega)$  becomes also static.

The generalized Loschmidt amplitude on the other hand stays a dynamic quantity also after the pulse is over. However, given that

$$\int dD L_{\hat{H}\hat{D}}^{|\psi(t)\rangle}(\omega, D) = 2\pi L(t, \omega) \quad (24)$$

there can only be dynamics with respect to  $D$ . In other words, there can be redistribution of spectral weight along the  $EV(\hat{D})$ -axis but not along the  $EV(\hat{H})$ -axis after the pulse. Hence, if after the pulse there is an overall trend to a redistribution of spectral weight towards larger double occupancy values we witness impact ionization. From our generalization of the Loschmidt amplitude one can tell which energy-states are responsible for the double-occupancy dynamics. This reflects that the generalized Loschmidt amplitude is a spectral decomposition with respect to two operators at the same time.

We find for all the systems under consideration that the single-photon excitations ( $EV(\hat{H}) \approx \omega_p$ ) predominately consist of  $EV(\hat{D}) = 1$  and 2 and the double-photon excitations of  $EV(\hat{D}) = 2$  and 3. The  $4 \times 3$  and  $6 \times 2$  systems show impact ionization (seen also in Ref. 10 in the rise of the double occupancy as a function of time). This finding is well captured by the generalized Loschmidt amplitude in Fig. 6(b)-(c), where we show a difference between the  $\Re L_{\hat{H}\hat{D}}$  shortly after the pulse (at  $t = t_p + 3\sigma_p = 14$ ) and at a much later time ( $t = 100$ ). We see that for the same energy eigenstates the number of double occupancies increases. The strongest change in the double occupation comes from the energy states at double-photon excitations ( $EV(\hat{H}) \approx 22$ ) or even triple-photon excitations ( $EV(\hat{H}) \approx 33$ ) and not from single-photon excitations. This behavior depends on the concrete system under consideration. In the  $4 \times 2$  Hubbard cluster also single-photon excitations have a significant contribution to the impact ionization (see Fig. 13 in the Appendix A).

An inverse effect to impact ionization (impact deionization) can be seen in the double occupation dynamics of the frustrated  $12 \times 1$  system shown in Fig. 6(f). Here the single and the double-photon excitations are of importance to the dynamics. However, the generalized Loschmidt here reveals a decrease of double occupations.

For the 12-site chains with only NN hopping and OBC or PBC (Fig. 6 (d)-(e) there is no net increase in the double occupancy between  $t = 14$  and  $t = 100$ . There is however still strong dynamics of the double occupancy visible. For example for  $12 \times 1$  in Fig. 6(d) we see at  $EV(\hat{H}) \approx 23.5$  a reduction of double occupancy whereas at  $EV(\hat{H}) \approx 22.8$  there is an increase. Summing up all contributions gives a cancellation and there is no overall increase in double occupation (which can be interpreted as effectively no impact ionization). This was also found to be the case in Ref. [10], where the time dependence of double occupancy after the pulse was shown for precisely the same systems and parameters as in our work.

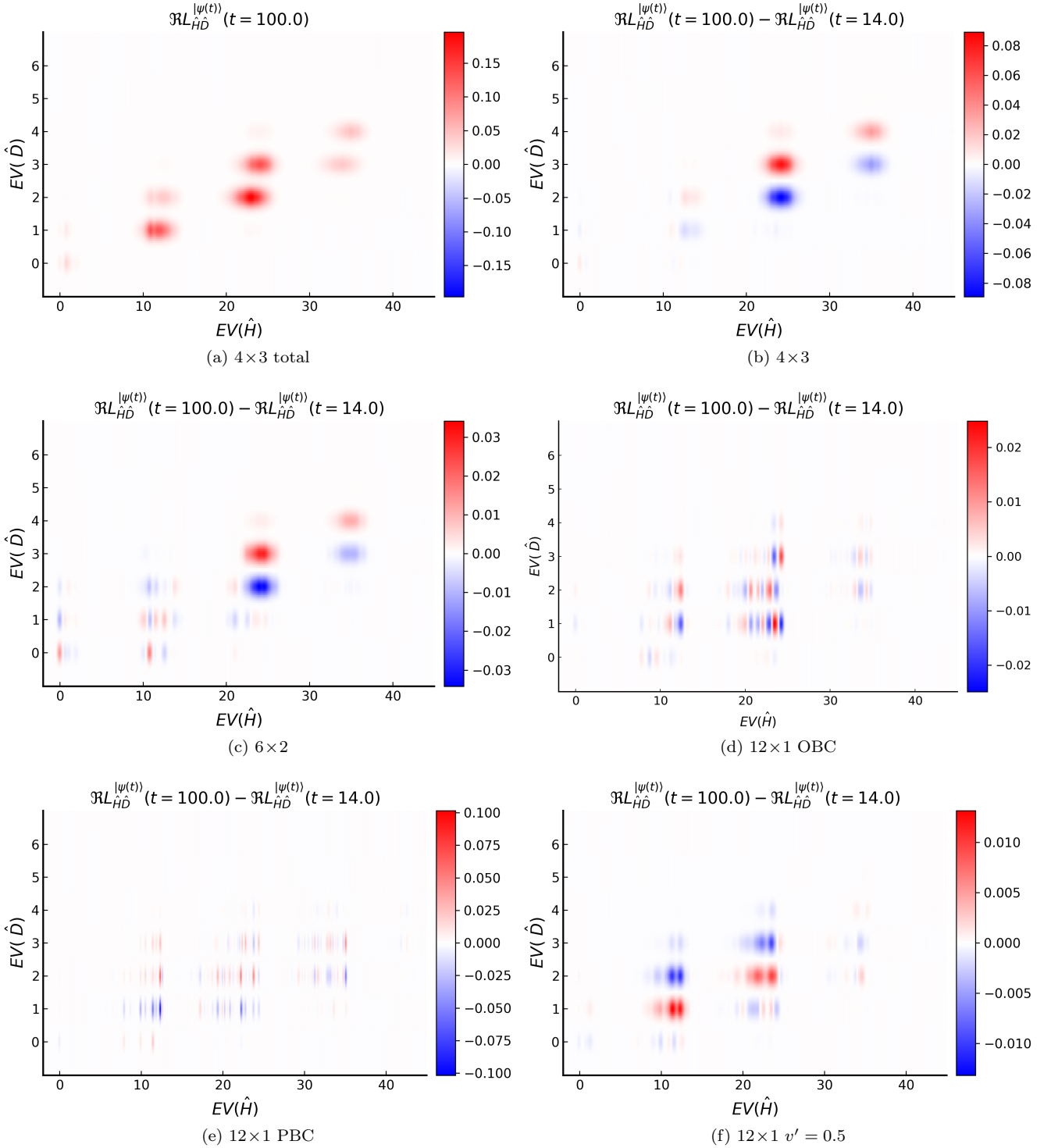


FIG. 6. Generalized Loschmidt amplitude for the  $N_s = 12$  site systems, allowing us better analyze the dynamics of the double occupations. In (a) the real part of  $L_{\hat{H}\hat{D}}^{|\psi(t)\rangle}$  is shown for  $t = 100$ . Plots (b)-(f) show the difference between  $L_{\hat{H}\hat{D}}^{|\psi(t)\rangle}$  long after the pulse ( $t = 100$ ) and shortly after the pulse ( $t = 14$ ). For all systems shown a consistent energy broadening of  $\sigma_\omega = 0.18$  and double occupancy eigenvalue broadening of  $\sigma_d = 0.1$  has been employed.

## VI. SPIN EXCITATIONS

In the following we investigate the influence of spin fluctuations on the dynamics of systems after a light pulse. It was shown in Ref. [10] that disorder as well as next-nearest-neighbor hopping enhances impact ionization in small Hubbard clusters. Moreover, one-dimensional chains do not show any significant impact ionization. This suggested that if a system has the tendency to order magnetically, excess kinetic energy may first break up this order or fluctuations, i.e. excess energy is transferred to magnons or paramagnons. This could be detrimental to impact ionization. To verify this proposition we investigate the spin-spin correlation function

$$C_{ij}(t, t') = \langle \hat{S}_z^i(t) \hat{S}_z^j(t') \rangle, \quad (25)$$

where in our units  $\hat{S}_z^i = \frac{1}{2}(\hat{n}_i^+ - \hat{n}_i^-)$ ; as well as the corresponding Kubo susceptibility

$$\begin{aligned} \chi_{ij}^R(t, t') &= -i\theta(t - t') \langle [\hat{S}_z^i(t), \hat{S}_z^j(t')] \rangle \\ &= 2\theta(t - t') \Im C_{ij}(t, t'). \end{aligned} \quad (26)$$

Furthermore, as a measure of the tendency for spin-order we also consider the expectation value of the Heisenberg Hamiltonian

$$E_H(t) = \langle \psi(t) | \hat{H}_H | \psi(t) \rangle \quad (27)$$

with

$$\hat{H}_H = \sum_{i>j} J_{ij} \left( \hat{S}_x^i \hat{S}_x^j + \hat{S}_y^i \hat{S}_y^j + \hat{S}_z^i \hat{S}_z^j \right). \quad (28)$$

This is motivated by the fact that in the limit of large interaction values  $U$ , the (static) Hubbard model can be mapped onto the Heisenberg model by the Schrieffer-Wolff transformation (see e.g [32, Chapter 2.2]). The spins at site  $i$  and  $j$  couple due to super-exchange with a coupling constant given by  $J_{ij} = 4\frac{v_{ij}^2}{U}$ . In Eq. (28) all three terms give the same contribution due to  $SU(2)$  symmetry. We utilized this fact to speed up the calculations. Although the Schieffer-Wolff mapping is far from being exact for  $U = 8$  used in this paper, it gives nonetheless an intuitive understanding of the properties of the Hubbard clusters. For example for  $J > 0$  (for NN-hopping) neighboring spins can lower  $E_H$  by aligning antiparallelly.

### 1. Spin susceptibility

We first consider the dynamic spin susceptibility in equilibrium. In Fig. 7, we show the  $\Im \chi^R(q, \omega)$  for the  $12 \times 1$  systems with PBC (upper panel) and OBC (lower panel). The double-wing structure of the paramagnon dispersion relation  $\propto |\sin(q)|$  is clearly visible [33]. The gap at  $q = \pi$  is system-size dependent. It is equal to  $J$  for a Hubbard dimer and vanishes for an infinitely large system. At  $q = 0$  the imaginary part of the susceptibility

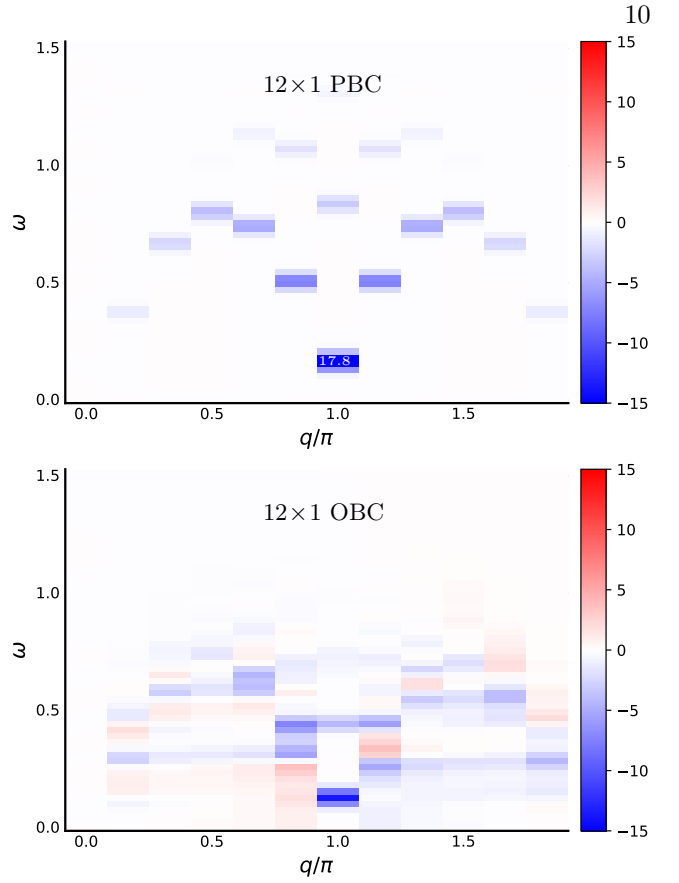


FIG. 7. Spin susceptibility  $\Im \chi^R(q, \omega)$  for a  $12 \times 1$  system with PBC (top) and OBC (bottom). For PBC the maximal absolute value  $\max |\Im \chi(q = \pi, \omega)| = 17.8$  is outside the colorbar and instead labeled explicitly to increase the visibility of the dispersion relation.

is exactly zero because the total spin in the system is a conserved quantity. For OBC the momentum  $q$  is no longer a good quantum number and  $\Im \chi(q, \omega)$  changes sign [34]. Nonetheless, also for this case one can still find a resemblance to the paramagnon dispersion relation similar to the case of PBC. The spin susceptibility is still quite large, but of course smaller than for the PBC. In both cases, the  $\omega$ - $q$  dispersion has an amplitude  $\sim J = 4v_{ij}^2/U = 0.5$ , and the finite-size spin gap is small enough ( $\sim 0.1$ ) for excess kinetic energy to be transferred to the spin system.

### 2. Spin-spin correlation function

The time-dependent equal time ( $t = t'$ ) spin-spin correlation functions  $\langle \hat{S}_z^1 \hat{S}_z^2 \rangle(t)$  for the 12-site clusters are shown in Fig. 8. For the ground states ( $t = 0$ ) of all investigated clusters, strong antiferromagnetic correlations are visible over several lattice sites (see also insets of Fig. 8). For the  $12 \times 1$  system with  $v' = 0.5$ , Fig. 8(e), the spins are frustrated which leads to a slightly smaller correlation length. After the light pulse the correlation length

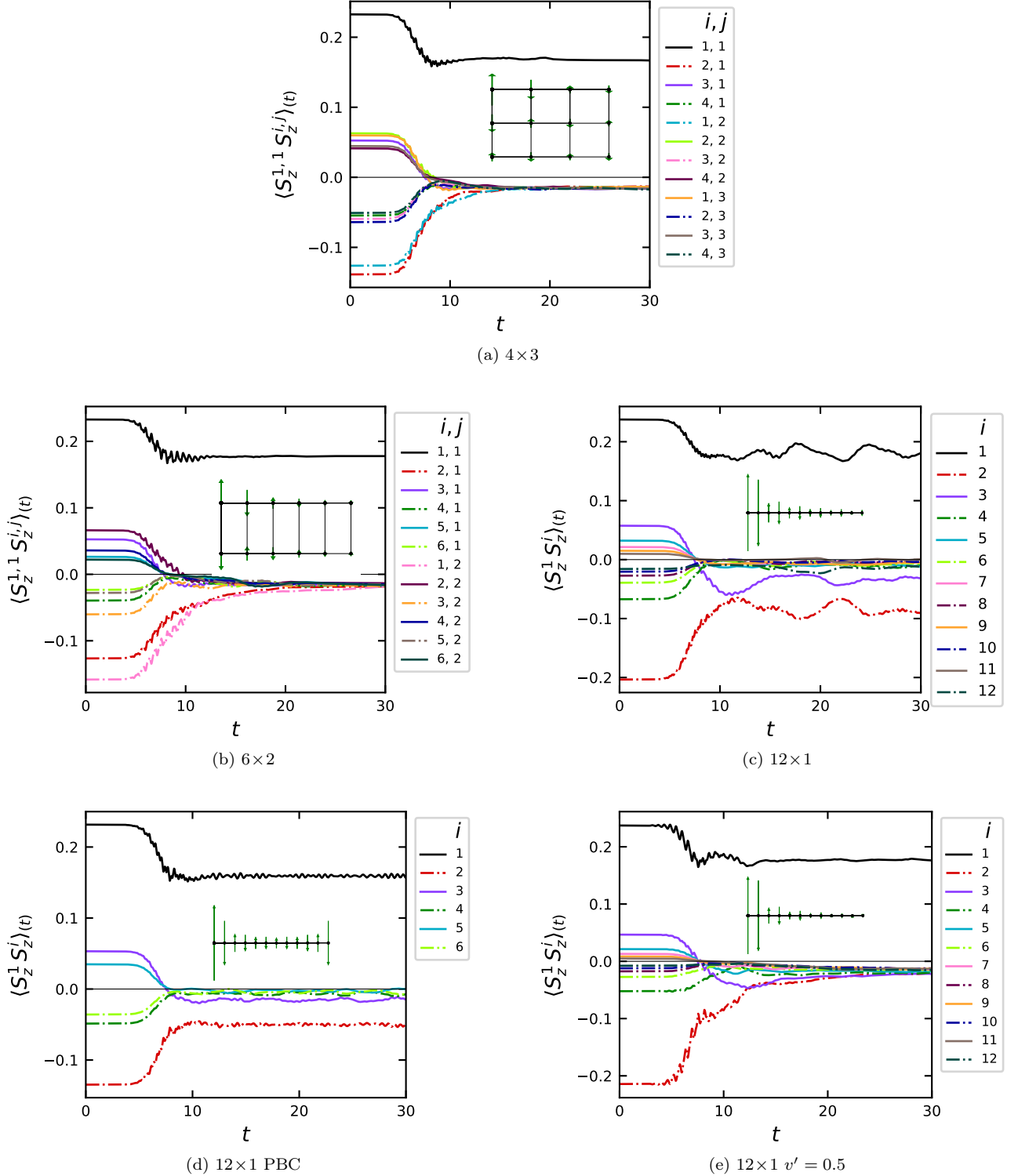


FIG. 8. Equal time spin correlation functions  $\langle \hat{S}_z^{1,1} \hat{S}_z^{i,j} \rangle(t)$  (for box geometries) and  $\langle \hat{S}_z^1 \hat{S}_z^i \rangle(t)$  (for chains), with the first spin operator kept fixed at the upper left site. In all plots different colors denote different sites for the second spin operator. In case of chains (c)-(e) one index  $j$  is enough. For box geometries (a,b) a pair of indices  $i$  and  $j$  is used to denote on which site the second operator is placed. Insets: The values for  $t = 0$  plotted as green arrows with the length proportional to the magnitude of the correlation function.

decreased significantly in all systems. For the  $4 \times 3$ ,  $6 \times 2$ , Fig. 8(a-b), and  $12 \times 1$   $v' = 0.5$ , Fig. 8(e), cases no tendency toward spin order survives the pulse. For  $12 \times 1$   $v' = 0$ , Fig. 8(c), and  $12 \times 1$  PBC, Fig. 8(d), systems the spins at neighboring sites are still correlated antiferromagnetically, but far less than before the pulse. The light pulse is strong enough to destroy long range spin correlations in all the considered Hubbard clusters.

### 3. Energy of the spin system

To assess the importance of energy absorbed by the spin system, we show in Fig. 9c the Heisenberg spin energy  $E_H$  defined in Eq. (27). We compare it to the total energy  $E_{\text{tot}}$ , the potential energy related to the double occupancy  $E_{\text{docc}}$  and the kinetic energy  $E_{\text{kin}}$  shown in Fig. 9 (a-b,d). They are defined as

$$\begin{aligned} E_{\text{tot}}(t) &= \langle \psi(t) | \hat{H}(t) | \psi(t) \rangle \\ E_{\text{docc}}(t) &= U \sum_i \langle \psi(t) | \hat{n}_{i\downarrow} \hat{n}_{i\uparrow} | \psi(t) \rangle \\ E_{\text{kin}}(t) &= \sum_{\sigma} \sum_{i \neq j} v_{ij}(t) \langle \psi(t) | \hat{c}_{j\sigma}^{\dagger} \hat{c}_{i\sigma} | \psi(t) \rangle. \end{aligned} \quad (29)$$

By definition  $E_{\text{tot}}(t) = E_{\text{kin}}(t) + E_{\text{docc}}(t)$ . In Fig. 9 the total energy at  $t = 0$  (the ground state energy in our case) was set to zero.

In all systems the additional energy coming from the  $E$ -field is leading to a rise in both kinetic and potential energy. After the pulse is over the total energy of the systems does not change any more. We can see that all 12-site systems considered absorb a similar amount of total energy, see Fig. 9 (d). In the  $4 \times 3$  and  $6 \times 2$  systems the double occupancy, and thus also  $E_{\text{docc}}$ , rises after the pulse due to impact ionization, which is consistent with Fig. 6. The frustrated  $12 \times 1$  chain with  $v' = 0.5$  shows a slight decrease of  $E_{\text{docc}}$  instead. The other two systems with a  $12 \times 1$  geometry do not show any systematic change in  $E_{\text{docc}}$ .

Comparing the time dependence of  $E_{\text{docc}}$  to  $E_H$  we do not see the anti-correlation anticipated in Ref. 10. Instead, we find an additional rise after the pulse in  $E_H$  for the  $6 \times 2$ ,  $4 \times 3$ ,  $12 \times 1$   $v' = 0.5$ , whereas the systems that still remained antiferromagnetically correlated after the pulse ( $12 \times 1$  PBC and OBC with  $v' = 0$ ) do not show any systematic change in  $E_H$ . We also see in Fig. 9 that  $E_H$  and its changes are significantly smaller than the other involved energies. From these considerations the supposition [10] that strong spin correlations prevent impact ionization in 12-site clusters does not seem to be confirmed. The two 12-site chains with NN-hopping remain however distinct in that they absorb less energy into the spin system. This is consistent with Fig. 8, where only for these systems the antiferromagnetic correlations survived the pulse.

## VII. GENERALIZED LOSCHMIDT AMPLITUDE FOR HEISENBERG AND TOTAL ENERGY

We now apply the generalized Loschmidt amplitude as defined in Eq. (21) to the spin-correlation energy (Heisenberg energy defined in Eq. (27)) and total energy, i.e. we take  $\hat{A} = \hat{H}(0)$  and  $\hat{B} = \hat{H}_H$ . In Fig. 10(a) we show the real part of the generalized Loschmidt amplitude  $L_{\hat{H}\hat{H}_H}$  for the  $4 \times 3$  system at a time long after the pulse ( $t = 100$ ). The system is brought so strongly out of equilibrium that the ground state contribution is almost negligible. The dynamics is dominated by the single- and double-photon excitations. Both give similar eigenvalue contributions for the Heisenberg energy, because the spin energy is small compared to the other energy scales (see Fig. 9). We observe the same for the other 12-site clusters (not shown here). In Figs. 10(b)-(f) we show the difference between  $L_{\hat{H}\hat{H}_H}$  at  $t = 100$  and at a shorter time after the pulse  $t = 14$  for all 12-site systems considered (analogously as in Fig. 6).

The first system, the  $4 \times 3$  geometry, is shown in Fig. 10(b). We find that the double-photon excitations ( $EV(\hat{H}) \approx 2\omega_p$ ) have almost no effect on the overall expectation value of  $E_H$  though there is some internal dynamic. There is a redistribution between the spin-energies  $\approx 0$  to larger but also to smaller values which cancel each other. The major states responsible for the long time trend in  $E_H$  for the  $4 \times 3$  system (cf. Fig. 9c) are the single-photon ( $EV(\hat{H}) \approx \omega_p$ ) excitations.

The situation is slightly different for the  $6 \times 2$  and the  $12 \times 1$   $v' = 0.5$  systems (Fig. 10(c) and (f), respectively). Here also the double-photon excitations show a clear trend towards further reordering of the spins and increasing the Heisenberg spin energy. For these systems both the single- and the double-photon excitations give important contributions to the long time behavior of  $E_H$ . In all three systems, where  $E_H$  increases long after the pulse, it is also clearly visible in the generalized Loschmidt amplitude  $L_{\hat{H}\hat{H}_H}$  [Figs. 10(b), (c), and (f)] as an increase in the contribution of states with higher eigenvalues of  $\hat{H}_H$ .

For the  $12 \times 1$  systems with PBC and OBC with only NN-hopping ( $v' = 0$ ) the situation is very different. Neighboring contributions regarding  $EV(\hat{H}_H)$ , which differ by a single spin flip, are alternating in sign [see Fig. 6(d-e)]. All the (slow) dynamics within the same  $EV(\hat{H})$  almost cancels out. This can also be seen in Fig. 9c. The remaining dynamic is on a shorter time scale and thus must be due to larger energy differences, i.e. between the different numbers of photoexcitations. The major contribution comes from the energy difference between the single- (and also double-)photon excitations and the ground state. This explains why the fluctuations in Fig. 9c have a frequency of  $\omega_p$  or  $2\omega_p$ .

Looking at Figs. 6 and 10 together, one observes that for three of the systems,  $4 \times 3$ ,  $6 \times 2$ , and  $12 \times 1$  with

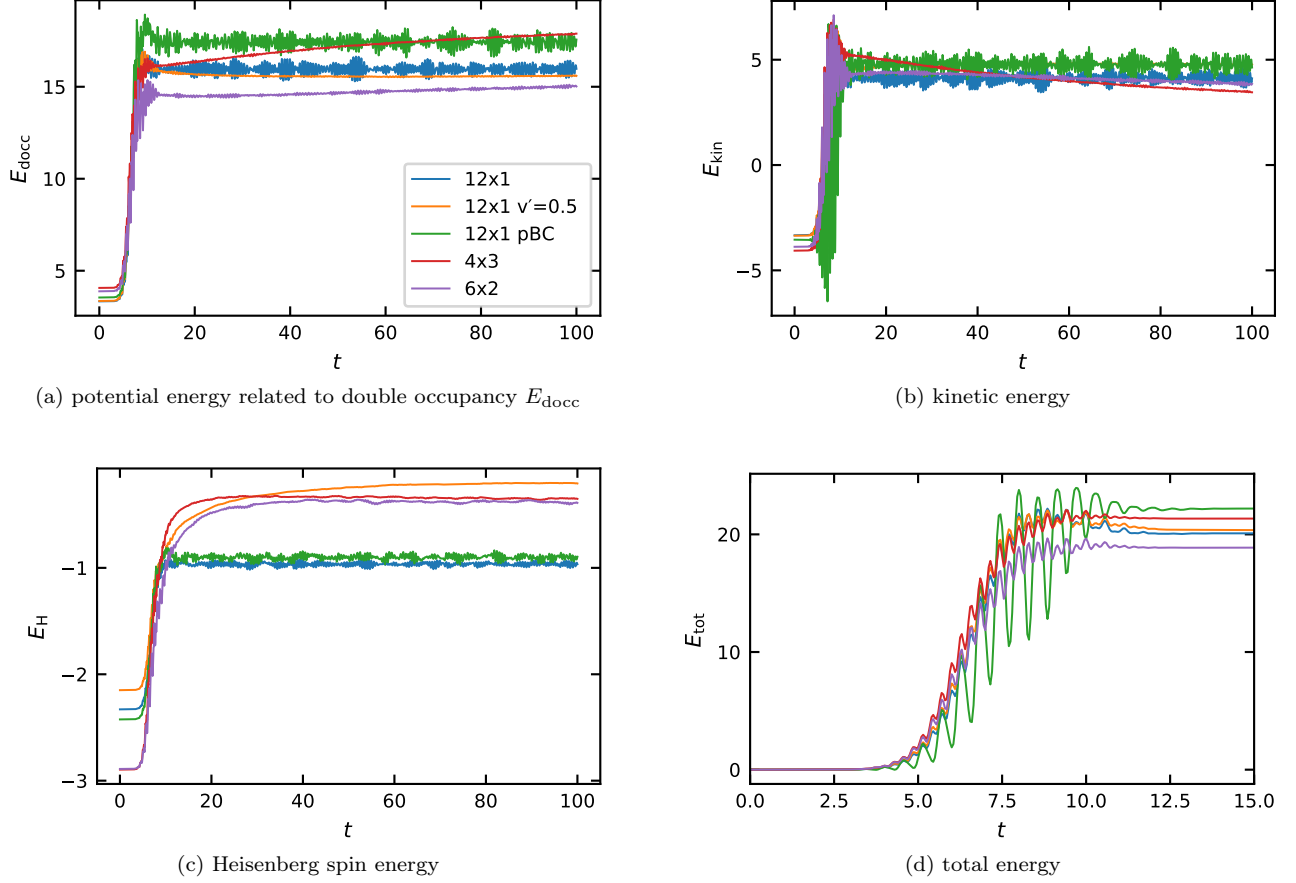


FIG. 9. Different contributions to the total energy of 12-site clusters, as defined in Eq. (27) and Eq. (29), as a function of time: (a) potential energy related to double occupancy  $E_{\text{docc}}$ ; (b) kinetic energy; (c) Heisenberg spin energy; and (d) total energy. Different colors correspond to different cluster geometries, as denoted in the legend in (a). Please note, that the total energy in (d) does not change after the pulse (centered at  $t_p = 8$ ) is over and therefore it is shown only for shorter times. The ground state energy corresponding to  $E_{\text{tot}}(t = 0)$  was set to zero. Parameters as described in Section II C.

$v' = 0.5$ , there is a clear tendency in the dynamics of the charge and spin excitations after the pulse is over. The contribution of higher eigenvalues of  $\hat{H}_{\text{H}}$  increases (i.e. the spin order is further destroyed) and the double occupancy either increases ( $4 \times 3$  and  $6 \times 2$ ) or slightly decreases ( $12 \times 1$  with  $v' = 0.5$ ). In the remaining two 12-site chains with NN-hopping only, there is no clear tendency in the dynamics and different contributions to double occupancy and spin energy cancel each other. The residual antiferromagnetic correlation (cf. Fig. 8) is not further destroyed and there is also no net increase or decrease in double occupancy.

## VIII. CONCLUSIONS

We presented the analysis of the dynamics of small Hubbard clusters during and after a photoexcitation with a strong electric pulse, focusing on 12-site systems with and without impact ionization. To this end we

applied novel commutator free Magnus integrators [25] for the time evolution (solution of the time-dependent Schrödinger equation).

The energies where the system can absorb energy (at initial times) can be accurately predicted from the Loschmidt amplitude  $L^{\hat{j}|\psi_0\rangle}$  also for a large electric field. For small fields our results reduce to the Fermi's golden rule. On the other hand, the description of optical absorption through the one-particle Green's function turns out to fail for purely one-dimensional systems. Here vertex corrections play the dominant role. This situation changes when the geometry of the system is changed to a box or a further neighbor hopping is added, increasing the coordination number. There the one-particle based 'bubble' contribution already qualitatively resembles the full result and in particular reproduces the correct optical gap.

We further generalized the Loschmidt amplitude to gain insights which energy states are responsible for the long time dynamics of the system. Specifically we ap-

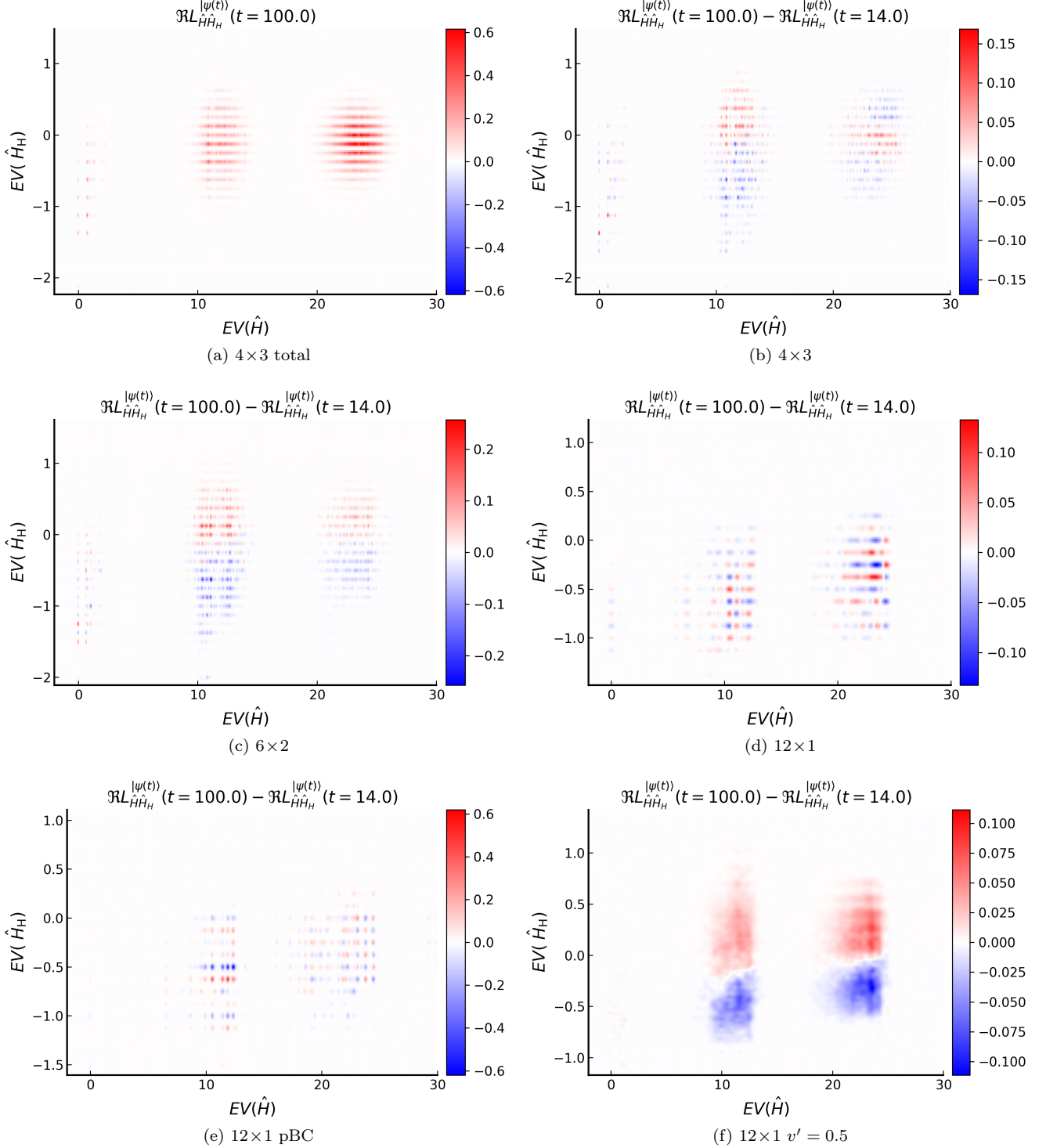


FIG. 10. Generalized Loschmidt amplitude for the  $N_s = 12$  site systems. In (a) the full generalized Loschmidt amplitude is given, in (b-f) relative change (differences) after the the pulse is over are shown.  $EV(\hat{H})$  broadening is  $\sigma_\omega = 0.18$ ;  $EV(\hat{H}_H)$  broadening  $\sigma_\omega = 0.02$ .

plied it first to the double occupancy. We found that for all the 12-site clusters we considered the impact ionization, if seen for times long after the pulse, originates predominantly from the double-photon excitations. Although we suspect that this is likely a consequence of the large strength of the electric field used in our study, our result for weaker fields (not shown in this paper) are inconclusive in this respect. The reason is that for weaker fields the generalized Loschmidt amplitude fluctuates (relatively) much stronger in time.

The spin dynamics of the 12-site systems, as reflected in spin-spin correlation functions and in the Heisenberg spin energy, does not confirm the expectations of Ref. [10], namely that spin-reordering tendencies might be detrimental to impact ionization. There was an increase in the Heisenberg spin energy for those systems that also displayed impact ionization. Furthermore the energy scales associated with the spin order were shown to be small compared to the other involved energy scales. Also the generalized Loschmidt amplitude applied to Heisenberg spin-energy did not show any clear anticorrelation between creating more double occupancies and spin excitations.

From a more general perspective, we have introduced a new analysis tool for studying the dynamics out of equilibrium: the generalized Loschmidt amplitude. We have applied it to study the dynamics of impact ionization in small Hubbard clusters after a light pulse. The generalized Loschmidt amplitude can also be employed to other physical problem and provides a computationally efficient way for getting a detailed picture of the nonequilibrium dynamics.

*Acknowledgments.* We thank O. Koch and W. Auzinger for many fruitful discussions. This work was supported by the Austrian Science Fund (FWF) through project P 30819. Calculations have been done on the Vienna Scientific Cluster (VSC).

## Appendix A: Properties of Loschmidt Amplitude

A one-operator Loschmidt amplitude may be defined for the hermitian operator  $\hat{A} = \hat{A}^\dagger$  as

$$L_A^{|\psi\rangle}(\bar{\alpha}) = \langle \psi | e^{-i\bar{\alpha}\hat{A}} | \psi \rangle,$$

from which it directly follows that

$$L_A^{|\psi\rangle}(\bar{\alpha})^* = L_A^{|\psi\rangle}(-\bar{\alpha})$$

and that it's Fourier transform  $L_A^{|\psi\rangle}(\alpha)$  is a real positive quantity. The normalization is for our Fouriertransform convention given by  $2\pi$ . Hence,  $\frac{1}{2\pi}L_A^{|\psi\rangle}(\alpha)$  fulfills the properties of a probability distribution. For the case where  $\hat{A} = \hat{H}$  the Loschmidt-amplitude gives the spectral decomposition of the state  $|\psi\rangle$  with respect to the possible eigenstates of the Hamiltonian. As this is the most important case we here dropped the subscript  $H$  in

the notation, and use  $L^{|\psi\rangle}(\omega)$  (instead of  $L_H^{|\psi\rangle}(\omega)$ ). If the groundstate energy of the Hamiltonian is chosen to be 0 (as for all calculations presented) one moreover has the property that  $L^{|\psi\rangle}(\omega < 0) = 0$ .

The one-operator Loschmidt amplitude can also be expressed in terms of the two-operator Loschmidt amplitude by integration

$$L_{\hat{A}}^{|\psi\rangle}(\alpha) = \frac{1}{2\pi} \int_{-\infty}^{\infty} d\beta L_{\hat{A}\hat{B}}^{|\psi\rangle}(\alpha, \beta). \quad (\text{A1})$$

It moreover fulfills the property

$$\langle \hat{A}^n \hat{B}^m \rangle = \frac{1}{(2\pi)^2} \int_{-\infty}^{\infty} d\alpha d\beta \alpha^n \beta^m L_{\hat{A}\hat{B}}^{|\psi\rangle}(\alpha, \beta). \quad (\text{A2})$$

just as it fulfills for the standard Loschmidt amplitude

$$\langle \hat{A}^n \rangle = \int_{-\infty}^{\infty} d\alpha \frac{1}{2\pi} \alpha^n L_{\hat{A}}^{|\psi\rangle}(\alpha). \quad (\text{A3})$$

While the one-operator Loschmidt amplitude is real,  $L_{\hat{A}}^{|\psi\rangle}(\alpha) \in \mathbb{R}$  the two operator variant can have an imaginary part as well (as  $[\hat{A}, \hat{B}] \neq 0$  in general). For Eq. (A2) only the real part gives a contribution, and the imaginary part vanishes. Therefor it is sufficient to only consider the real part of the Fourier transformed two-operator Loschmidt amplitude.

*Expression in terms of projectors* – For some operators the possible eigenvalues as well as the corresponding projectors  $P$  can be computed cheaply without the need to diagonalize a large matrix numerically. For example the double occupancy operator  $\hat{D} = \sum_i \hat{n}_{\downarrow i} \hat{n}_{\uparrow i}$  has for a half-filled system with  $N_s$  sites the eigenvalues  $\{0, 1, \dots, N_s/2\}$ . [35] In such a case it is convenient to express (and calculate numerically) the Loschmidt amplitude by means of these projectors (e.g.  $\hat{B} = \sum_b b |b\rangle \langle b| = \sum_b b \hat{P}_b$ ). A convenient way of expressing the Loschmidt amplitude via one operator  $\hat{A}$  where the eigenspectrum is a-priori unknown, and one operator  $\hat{B}$  where the projectors as well as the eigenspectrum is well known is given by

$$\begin{aligned} P_b L_{\hat{A}}^{|\psi(t)\rangle}(\bar{\alpha}) &= \langle \psi(t) | \hat{P}_b e^{-i\bar{\alpha}\hat{A}} | \psi(t) \rangle \\ P_b L_{\hat{A}}^{|\psi(t)\rangle}(\alpha) &= 2\pi \langle \psi(t) | \hat{P}_b |a\rangle \langle a | \psi(t) \rangle \end{aligned} \quad (\text{A4})$$

The set of functions for all  $b$  has exactly the same information content as Eq. (21) but it is cheaper to compute.

*Relation to the optical conductivity* – The Loschmidt amplitude of  $|\psi\rangle = \hat{j}|\psi_0\rangle$  is related to the retarded current-current correlation function as

$$\begin{aligned} K^R(t, 0) &= i\theta(t) \langle [\hat{j}(t), \hat{j}(0)] \rangle_0 \\ &= -2\theta(t) \Im L^{|\psi\rangle}(t). \end{aligned} \quad (\text{A5})$$

For convenience we also introduce the current-current correlation function as  $K(t) = i \langle [\hat{j}(t), \hat{j}(0)] \rangle_0$ .

In frequencies this amounts to

$$L^{\hat{j}|\psi\rangle_0}(\omega > 0) = 2 \Im K^R(\omega > 0). \quad (\text{A6})$$

Eq. (A6) can be proven as follows: We start by separating the Loschmidt amplitude into a symmetric and an anti-symmetric part.

$$L^{\hat{j}|\psi\rangle_0}(\omega) \equiv \frac{1}{2} L^{\hat{j}|\psi\rangle_0}^s(\omega) + \frac{1}{2} L^{\hat{j}|\psi\rangle_0}^a(\omega). \quad (\text{A7})$$

By definition

$$\begin{aligned} L^{\hat{j}|\psi\rangle_0}^s(\omega) &= L^{\hat{j}|\psi\rangle_0}^s(-\omega) \\ L^{\hat{j}|\psi\rangle_0}^a(\omega) &= -L^{\hat{j}|\psi\rangle_0}^a(-\omega). \end{aligned} \quad (\text{A8})$$

Because  $L^{\hat{j}|\psi\rangle_0}(\omega) \in \mathbb{R}$  (cf. Eq. (12)) for  $\omega > 0$  and  $\omega < 0$ , also  $L^{\hat{j}|\psi\rangle_0}^s(\omega) \in \mathbb{R}$  and  $L^{\hat{j}|\psi\rangle_0}^a(\omega) \in \mathbb{R}$ . We further use that because  $L^{\hat{j}|\psi\rangle_0}(\omega < 0) = 0$  (groundstate energy is chosen as zero) the symmetric part must cancel the anti-symmetric part for negative frequencies. Due to their respective (anti-)symmetry it follows that for positive frequencies they both must equal the full function

$$L^{\hat{j}|\psi\rangle_0}(\omega > 0) = L^{\hat{j}|\psi\rangle_0}^s(\omega > 0) = L^{\hat{j}|\psi\rangle_0}^a(\omega > 0). \quad (\text{A9})$$

The corresponding Fourier transforms are purely real/imaginary. As a next step consider

$$\begin{aligned} K(t) &= -2L^{\hat{j}|\psi\rangle_0}(t) \\ &= -2\Im \left( \frac{1}{2} L^{\hat{j}|\psi\rangle_0}^s(t) + \frac{1}{2} L^{\hat{j}|\psi\rangle_0}^a(t) \right) \\ &= -\Im L^{\hat{j}|\psi\rangle_0}^a(t) \\ &= iL^{\hat{j}|\psi\rangle_0}^a(t). \end{aligned} \quad (\text{A10})$$

The first line follows directly from the definition of  $L^{\hat{j}|\psi\rangle_0}(t)$ . In the second line Eq. (A7) was inserted. In the third line we used that  $L^{\hat{j}|\psi\rangle_0}^s(t)$  is purely real. In the last line we used that  $L^{\hat{j}|\psi\rangle_0}^a(t)$  is purely imaginary. In frequencies Eq. (A10) can also be written as

$$iL^{\hat{j}|\psi\rangle_0}^a(\omega) = K(\omega). \quad (\text{A11})$$

The last step is now to relate  $K(\omega)$  to  $\Im K^R(\omega)$ . This can be done by splitting up  $K(t) \in \mathbb{R}$  into a symmetric and an anti-symmetric part and using the fact that  $K(t) = -K(-t)$  is anti-symmetric in time. Thus the anti-symmetric part  $K^R a(t)$  is given by  $K(t)$ :

$$\begin{aligned} K^R(t) &\equiv \frac{1}{2} K^R s(t) + \frac{1}{2} K^R a(t) \\ &= \frac{1}{2} K^R s(t) + \frac{1}{2} K(t) \end{aligned} \quad (\text{A12})$$

Taking the imaginary part of the Fourier-transform of Eq. (A12) (and using  $K^R s(\omega) \in \mathbb{R}$ ) leads to

$$K(\omega) = 2i\Im K^R(\omega) \quad (\text{A13})$$

Inserting Eq. (A13) into Eq. (A11) gives

$$L^{\hat{j}|\psi\rangle_0}^a(\omega) = 2\Im K^R(\omega). \quad (\text{A14})$$

Thus using Eq. (A9) we have proven Eq. (A6).

## Appendix B: Equilibrium Green's function

In Fig. 11 we show the local spectral function  $A_{\text{avg, loc.}}(\omega)$  (averaged over sites) for all the 12-site systems considered in the main text. Since direct calculation in the Lehmann representation is unfeasible due to memory constraints,  $A(\omega)$  was obtained here by time propagation with the time-independent Hamiltonian. Since for finite systems the spectral function consists of a set of  $\delta$ -peaks, we used a Gaussian broadening of  $\sigma_\omega = 0.13$ .

For the systems we considered that were with NN hopping only, the spectral function is particle-hole symmetric. This is not the case in the 12-site chain with NNN hopping of  $v' = 0.5$  (as clearly seen in the Fig. 11).

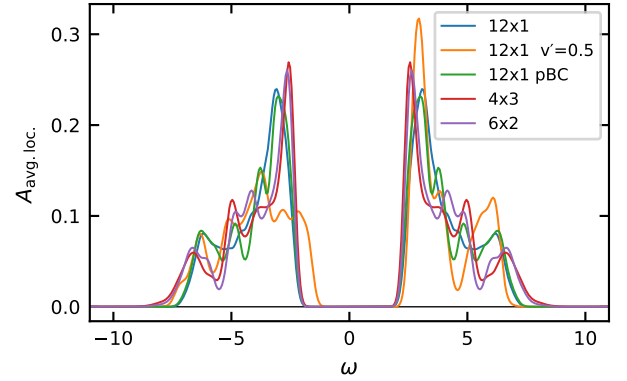


FIG. 11. Local average equilibrium Green's function for all considered  $N_s = 12$  systems. It is related to the retarded Green's function according to  $A_{\text{avg, loc.}}(\omega) = \frac{1}{N_s} \sum_i \frac{-1}{\pi} \Im G_{ii}^R(\omega)$ .

## Appendix C: Optical conductivity in strong-coupling

Figure 12 shows the Loschmidt amplitude/ optical conductivity for  $12 \times 1$  systems with periodic boundary conditions for different values of  $U$ . As a comparison also analytical results of Lyo et al. [29] in the large  $U$  limit are shown (dotted line). The peak structures are due to the different (relative) momentum values of the electron-hole pair created on a nearly antiferromagnetic background. In Ref. 29 the background (ground state) considered was antiferromagnetic, which is likely the cause of the difference in position of the peaks in the analytic and our results. Although we are close to the antiferromagnetic phase, we still have a paramagnetic (non-degenerate) ground state per construction.

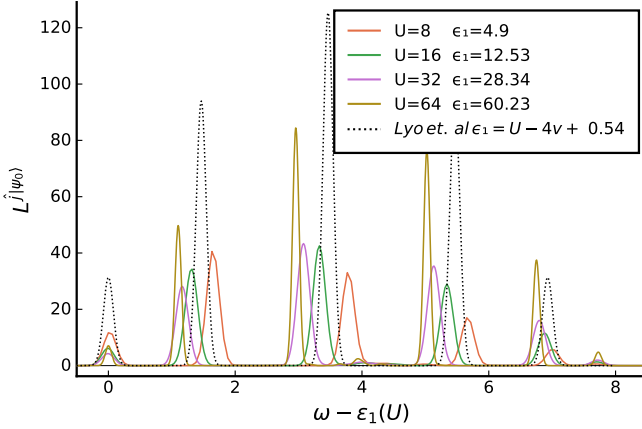


FIG. 12. Loschmidt amplitude  $L^j|\psi_0\rangle$  corresponding to  $2 \cdot \sigma^R(\omega) \cdot \omega$  for  $\omega > 0$  for the  $12 \times 1$  system with PBC.  $\epsilon_1$  corresponds to the lowest energy at which the system can absorb light and is always slightly larger than  $U - 4v$ . The analytical results of a large  $U$  expansion from Lyo et. al [29] are shown as the dotted line.

#### Appendix D: Generalized Loschmidt amplitude for a $4 \times 2$ system.

In Fig. 13 we show the generalized Loschmidt amplitude defined in Eq. (23) for a  $4 \times 2$  system. In this system significant contributions to impact ionization come from the single- and the double photon-excitations.

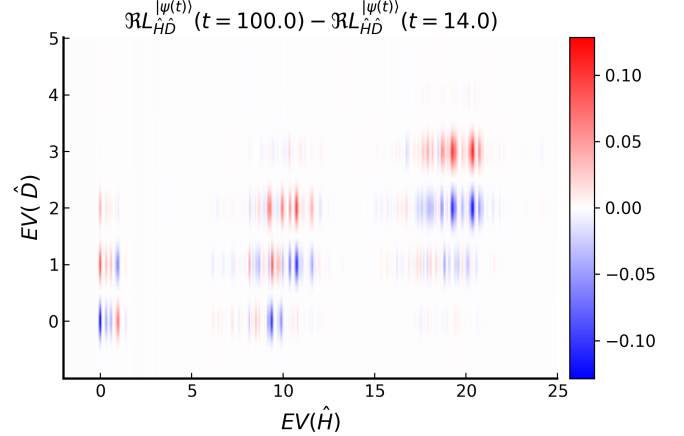


FIG. 13. Generalized Loschmidt amplitude for a  $4 \times 2$  system. The parameters are as in [10] namely  $U = 6$ ,  $a = 0.8$ ,  $\omega_p = 9$ . Impact ionization originates in this system also from single photon excitation.

---

[1] C. Giannetti, M. Capone, D. Fausti, M. Fabrizio, F. Parmigiani, and D. Mihailovic, *Adv. Phys.* **65**, 58 (2016).

[2] M. Zonno, F. Boschini, and A. Damascelli, *J. Electron. Spectrosc. Relat. Phenom.* **251**, 147091 (2021).

[3] E. Manousakis, *Phys. Rev. B* **82**, 125109 (2010).

[4] E. Assmann, P. Blaha, R. Laskowski, K. Held, S. Okamoto, and G. Sangiovanni, *Phys. Rev. Lett.* **110**, 078701 (2013).

[5] L. Wang, Y. Li, A. Bera, C. Ma, F. Jin, K. Yuan, W. Yin, A. David, W. Chen, W. Wu, W. Prellier, S. Wei, and T. Wu, *Phys. Rev. Applied* **3**, 064015 (2015).

[6] P. Werner, K. Held, and M. Eckstein, *Phys. Rev. B* **90**, 235102 (2014).

[7] M. E. Sorantin, A. Dorda, K. Held, and E. Arrigoni, *Phys. Rev. B* **97**, 115113 (2018).

[8] E. Manousakis, *Sci. Rep.* **9**, 20395 (2019).

[9] J. Holleman, M. M. Bishop, C. Garcia, J. S. R. Vellore Winfred, S. Lee, H. N. Lee, C. Beekman, E. Manousakis, and S. A. McGill, *Phys. Rev. B* **94**, 155129 (2016).

[10] A. Kauch, P. Worm, P. Prauhart, M. Innerberger, C. Watzenböck, and K. Held, *Phys. Rev. B* **102**, 245125 (2020).

[11] F. Maislinger and H. G. Evertz, [arXiv:2007.16201 \[cond-mat.str-el\]](https://arxiv.org/abs/2007.16201).

[12] M. Wais, J. Kaufmann, M. Battiato, and K. Held, *Phys. Rev. B* **103**, 205141 (2021).

[13] W. Shockley and H. J. Queisser, *J. Appl. Phys.* **32**, 510 (1961).

[14] H. Aoki, N. Tsuji, M. Eckstein, M. Kollar, T. Oka, and P. Werner, *Rev. Mod. Phys.* **86**, 779 (2014).

[15] A. Alvermann and H. Fehske, *J. Comput. Phys.* **230**, 5930 (2011).

[16] M. Innerberger, P. Worm, P. Prauhart, and A. Kauch, *Eur. Phys. J. Plus* **135**, 922 (2020).

[17] It is named after Loschmidt who in discussions with Boltzmann in Vienna raised the question of consistency between time irreversibility and the second law of thermodynamics (for a historical introduction see e.g. Refs. 36 and 37).

[18] M. Heyl, A. Polkovnikov, and S. Kehrein, *Phys. Rev. Lett.* **110**, 135704 (2013).

[19] M. Heyl, *EPL (Europhysics Letters)* **125**, 26001 (2019).

[20] C. Rylands and N. Andrei, *Phys. Rev. B* **99**, 085133 (2019).

[21] T. Pálmai and S. Sotiriadis, *Phys. Rev. E* **90**, 052102 (2014).

[22] E. L. Hahn, *Phys. Rev.* **80**, 580 (1950).

[23] J. Hubbard, *Proc. R. Soc. Lond. A* **276**, 238 (1963).

[24] R. Peierls, *Z. Phys.* **80**, 763 (1933).

[25] W. Auzinger, J. Dubois, K. Held, H. Hofstätter, T. Jawcki, A. Kauch, O. Koch, K. Kropielnicka, P. Singh, and C. Watzenböck, [arXiv:2104.02034 \[math.NA\]](https://arxiv.org/abs/2104.02034).

[26] Note that  $\hat{H}$  is isospectral in the Weyl gauge [25], meaning that its eigenvalues do not depend on time. This does, however, not mean that  $L^{|\psi\rangle}(\omega)$  is independent of the time at which  $\hat{H}(t)$  was evaluated.

[27] D. M. Kennes, C. Karrasch, and A. J. Millis, *Phys. Rev. B* **101**, 081106 (2020).

[28] The usual way to calculate the density of states would require a full diagonalization of the Hamiltonian and is thus only feasible for rather small system sizes. For the  $8 \times 1$  system  $\dim \mathcal{H} = \binom{8}{4}^2 = 4900$  this was possible and is shown in Fig. 2. For the various  $N_s = 12$  systems where  $\dim \mathcal{H} = \binom{12}{6}^2 = 853776$  the calculation of the density of states was unfeasible due to memory constraints.

[29] S. K. Lyo and J. P. Gallinar, *Journal of Physics C: Solid State Physics* **10**, 1693 (1977).

[30] J. Rammer, *Quantum Field Theory of Non-equilibrium States* (Cambridge University Press, 2007).

[31] J. Schwinger, *J. Math. Phys.* **2**, 407 (1961).

[32] A. Altland and B. Simons, *Condensed Matter Field Theory* (Cambridge University Press, 2006).

[33] S. Blundell, *Magnetism in Condensed Matter*, Oxford Master Series in Condensed Matter Physics (OUP Oxford, 2001).

[34] For PBC  $\sum_{R_i, R_j} \int_{-\infty}^{\infty} dt e^{-i\omega t} e^{-iq_1 R_i} e^{-iq_2 R_j} \chi_{R_i, R_j}^R(t) \propto \delta_{q_1, -q_2}$ . For OBC this is no longer the case. In Fig. 7 the diagonal parts  $\chi^R(q_1, \omega) := \chi^R(q_1, -q_1, \omega)$  are shown.

[35] The eigenstates of  $\hat{D}$  can also be computed efficiently by means of bit-shifts in the second-quantization basis.

[36] T. Gorin, T. Prosen, T. H. Seligman, and M. Žnidarič, *Phys. Rep.* **435**, 33 (2006).

[37] S. Brush, *Kinetic Theory* (Elsevier Pergamon Press, Headington Hill Hall, Oxford, 1966).